Neutrino-electron scattering and solar neutrino experiments

John N. Bahcall

Institute for Advanced Study, Princeton, New Jersey 08540

Neutrino-electron scattering experiments can elucidate the flavor content, spectrum shape, intensity, time dependence, and angular distribution of solar neutrinos. The author presents detailed calculations for all of the important solar neutrino sources of the predicted energy and angular dependence of the recoil electrons, as well as the total cross sections. In addition, the author discusses how neutrino-electron experiments can help distinguish between various proposed solutions of the solar neutrino problem.

CONTENTS

I. INTRODUCTION

How can we "solve" the solar neutrino problem? The number of proposed solutions is already large and is growing faster than the rate at which new experiments are being undertaken. We need to reverse this unfavorable ratio. The purpose of the present paper is to provide guidance in undertaking and interpreting solar neutrino experiments that are based upon neutrino-electron scattering.

In order to understand both the solar interior and neutrino propagation, we need to determine the *flavor* content, the *energy spectrum,* the *intensity,* and the *time dependence* of the neutrinos arriving at Earth. I will show in the following discussion that solar neutrino experiments involving neutrino-electron scattering can provide valuable information about all of these characteristics of the incident neutrinos. This detailed information will supplement the integral results obtained from radiochemical experiments [using, for example, ^{71}Ga (Barabanov *et al.*, 1985; Hampel, 1985), ^{81}Br (Hurst *et al.*, 1984), and ^{98}Mo (Cowan and Haxton, 1982)]. The radiochemical experiments are designed to determine whether the discrepancy between prediction and observation in the ^{37}Cl experiment (Bahcall and David, 1976) is caused by a lack of understanding of the solar interior or by new physics involved in neutrino propagation. The multiplicity of theoretical "solutions" has made it necessary to consider, in addition, experiments that are sensitive to neutrinos of different flavors and energies.

Neutrino-electron scattering has four features that are of diagnostic importance: (1) the electrons are primarily scattered forward in the direction connecting the Earth and the sun (Bahcall, 1964); (2) the shape of the recoil energy spectrum reflects the solar neutrino spectrum (Bahcall, 1964; Reines and Kropp, 1964); (3) the magnitude of the cross section is sensitive to neutrino flavor ('t Hooft, 1971); and (4) individual events can be electronically counted, thus giving high time resolution. The *angular distribution* (which is strongly peaked in the forward direction of the Earth-sun axis) allows one to determine experimentally whether the electrons come from the sun. The measured recoil energy spectrum can be used to test for consistency with the theoretical solar neutrino energy spectrum. One can infer the incoming neutrino flavor by exploiting the sensitivity of the magnitude of the scattering cross sections to neutrino type. By comparing the results of scattering experiments with absorption rates (involving charge-changing interactions only) measured in the ^{37}Cl and other radiochemical experiments, one can determine if neutrino oscillations (resonant or nonresonant) have occurred. The time resolution can distinguish between the steady-state fluxes expected from the solar core and time-dependent events on the solar surface or elsewhere (see the discussion in Davis, 1986). They may also be a diurnal modulation of the solar neutrino flux caused by resonance scattering in the Earth (see Dar *et al.*, 1986 and Cribier *et al.*, 1986).

In order to facilitate the planning and interpretation of solar neutrino experiments, I present total cross sections, angular distributions, and recoil energy spectra for the scattering of electrons by the solar neutrino sources with the largest expected fluxes (i.e., *p-p*, *p-e-p*, ^{7}Be, ^{8}Be, ^{13}N, and ^{15}O neutrinos; see Sec. II). In addition, I include calculations for the rare but relatively high-energy neutrinos produced by the $^{3}\mathrm{He} + p$ reaction. These results will be useful in analyzing experiments that are in progress, or are planned, including neutrino-electron scattering in water (Bakich and Peak, 1985), a heavy-water detector (Chen, 1985), a silicon bolometric detector (Cabrera, Krauss, and Wilczek, 1985), a liquid-argon detector (Bahcall, Baldo-Ceolin, Cline, and Rubbia, 1986) a scintillator experiment to measure ^{7}Be neutrinos (Mann, 1986), the scintillator detector for the ^{115}In experiment (Raghavan, 1978), and several proposals to use existing proton-decay detectors to observe solar neutrinos (cf. Arisaka *et al.*, 1985; Cline, 1985; Agiletta *et al.*, 1986).

Background effects are often the most difficult problem

in a solar neutrino experiment, but backgrounds usually decrease as the energy of the detected electron increases. Therefore, most of the discussion of electron-scattering detectors in the literature concentrates on the neutrinos from ^{8}B decay, which have energies up to 15 MeV. I compute the scattering cross sections for the crucial ^{8}B neutrinos using a recently derived neutrino spectrum (Bahcall and Holstein, 1986) that accurately takes account of the shape of the broad excited state to which ^{8}B decays. The shape was determined using a detailed measured α-particle spectrum (Wilkinson and Alburger, 1971; Warburton, 1986) that results from the decay of ^{8}Be. The calculated spectrum of neutrinos from ^{8}B decay also takes account of forbidden corrections to the weak interactions (Bahcall and Holstein, 1986) as well as the more familiar allowed contributions for solar interior β-decay reactions (Bahcall, 1978).

Although they are even rarer in the standard solar model than the ^{8}B neutrinos, the neutrinos produced by the ^{3}He + p reaction [see Eq. (2) below] are also of special interest experimentally since they have a significantly higher end-point energy of 18.773 MeV.

A number of the planned experiments are expected to have good energy resolution, as well as some angular resolution for the recoil electrons. I have therefore derived the detailed spectra for the energy and angular distributions of the recoil electrons. In order to make the results directly applicable to the proposed solar neutrino experiments, the cross sections for the high-energy ^{8}B and ^{3}He + p neutrinos are presented as a function of the minimum energy $T_{\min}$ that the recoil electron must have to be counted.

I shall assume that, except where explicitly stated otherwise, the spectrum of solar neutrino energies is unchanged as the electron neutrinos travel from the central regions of the sun to the Earth. This assumption is valid, for most parameters of interest, even if the neutrinos undergo nonresonant oscillations in transit (Bahcall and Frautschi, 1969; Gribov and Pontecorvo, 1969). For comparative purposes, I have also computed the results if *all* of the electron neutrinos are converted to muon neutrinos within the sun or in transit from the sun to the Earth. The differences between the all-ν_e results and the all-ν_μ results represent an upper limit to the effects that can be anticipated from flavor-changing interactions. In a subsequent paper (Bahcall, Gelb, and Rosen, 1987) we present the detailed theoretical predictions that apply if resonant neutrino oscillations, the *MSW effect* (Mikheyev and Smirnov, 1986; Wolfenstein, 1978), change some of the electron neutrinos to muon neutrinos. Finally, I give the expected cross sections and spectra if neutrino *decay* (Bahcall, Cabibbo, and Yahil, 1972; Bahcall, Petcov, Toshev, and Valle, 1986) is the correct explanation of the "solar neutrino problem."

Most readers will want to skip around in this paper, looking initially at the figures and reading only those parts that are of special interest to them. To facilitate this shopping process, I provide the following guide to the contents of the paper. I describe the most important recognized solar neutrino sources in Sec. II; this section should be read quickly by everyone because it establishes the notation that is used throughout. I summarize in Sec. III the basic equations that are used in the numerical calculations; this section can be skipped by readers who are primarily interested in the applications. I give in Sec. IV (Table I) the total neutrino-electron scattering cross sections for all of the neutrino sources described in Sec. II and, for the higher-energy ^{8}B and ^{3}He + p neutrinos, I tabulate (in Tables II and III) the total cross sections as a function of the minimum accepted kinetic energy of the recoil electrons. These results are convenient for estimating expected event rates in various detectors. Because of their experimental importance, I provide in Sec. V the calculated recoil energy spectra that are produced by scattering of electrons by either ^{8}B or ^{3}He + p neutrinos (Tables IV–VIII), which are assumed to be either pure ν_e or pure ν_μ. The shapes of the recoil spectra are best appreciated when presented in gracphical form. I illustrate the expected recoil spectra from the p-p, p-e-p, ^{7}Be, ^{8}Be, and ^{3}He + p neutrinos in Figs. 3–7. I describe in Sec. VI the expected angular distributions. The results are illustrated in Figs. 8–10 and, for the high-energy neutrinos, in Table IX. I consider in Sec. VII the effect of neutrino decay on the total event rates (see especially Table X) and on the shape of the predicted spectrum of electron recoil energies (Figs. 12–14). The scattering cross sections for *specific* neutrino energies are given in Table XI and discussed in Sec. VIII. In Sec. IX, I summarize the main results and conclusions.

Many of the important references and much of the background of this study are contained in two earlier papers in the *Reviews of Modern Physics* (Bahcall, 1978; Bahcall, Heubner, Lubow, Parker, and Ulrich, 1982). The reader is referred to these two preceding papers (and to papers in AIP Conference Proceedings No. 126, to Bahcall and Davis, 1982; and to Davis, 1986) for basic information on the solar neutrino problem and on experiments that utilize (charge-changing) neutrino absorption.

II. NEUTRINO SOURCES AND SPECTRA

The most important reactions that are believed to produce solar neutrinos with continuous energy spectra are (Bahcall *et al.*, 1982; Bahcall and Ulrich, 1987)

$$p + p \rightarrow {}^2\mathrm{H} + e^+ + \nu_e \quad (\leq 0.4203 \text{ MeV}), \tag{1}$$

$$^3\mathrm{He} + p \rightarrow {}^4\mathrm{He} + e^+ + \nu_e \quad (\leq 18.773 \text{ MeV}), \tag{2}$$

$$^8\mathrm{B} \rightarrow {}^8\mathrm{Be}^* + e^+ + \nu_e \quad (\leq 15 \text{ MeV}), \tag{3}$$

$$^{13}\mathrm{N} \rightarrow {}^{13}\mathrm{C} + e^+ + \nu_e \quad (\leq 1.199 \text{ MeV}), \tag{4}$$

$$^{15}\mathrm{O} \rightarrow {}^{15}\mathrm{N} + e^+ + \nu_e \quad (\leq 1.732 \text{ MeV}), \tag{5}$$

and

$$^{17}\mathrm{F} \rightarrow {}^{17}\mathrm{O} + e^+ + \nu_e \quad (\leq 1.740 \text{ MeV}). \tag{6}$$

The numbers given in parentheses are, except for the ^{8}B

neutrinos of Eq. (3), the maximum neutrino energies for the individual reactions and are computed from the tabulated atomic mass differences. The continuous spectra used in the calculations of neutrino-electron scattering are computed as described in Bahcall (1978). The situation is more complicated for the important neutrinos from ^{8}B decay (cf. Sec. I). The state in ^{8}Be that is predominantly populated by the decay of ^{8}B is very broad; the neutrino spectrum in this case is computed from the measured α-particle spectrum that results from the decay of ^{8}Be.

Electron-capture reactions produce neutrino lines with discrete energies except for a small thermal broadening (of order of a few keV). The most important solar neutrino lines are

$$p+e^-+p\rightarrow{}^2\mathrm{H}+\nu_e \quad (1.442\ \mathrm{MeV}) \tag{7}$$

and

$$^7\mathrm{Be}+e^-\rightarrow{}^7\mathrm{Li}+\nu_e$$
$$(0.862\ \mathrm{MeV},\ 89.7\%,\ 0.384\ \mathrm{MeV},10.3\%)\ . \tag{8}$$

I shall use where convenient the (rhyming) abbreviations "hep" and "pep" to describe the neutrinos from the reactions (2) and (7).

III. BASIC RELATIONS

The differential cross section for producing a recoil electron with kinetic energy T by scattering with a neutrino of initial energy q is ('t Hooft, 1971)

$$\frac{d\sigma}{dT}=\sigma_0[g_L^2+g_R^2(1-T/q)^2-g_Lg_R(T/q^2)]\ , \tag{9}$$

where

$$g_L=(\pm\tfrac{1}{2}+\sin^2\theta_W),\quad g_R=\sin^2\theta_W\ . \tag{10}$$

The upper sign applies for ν_e-e^- scattering and the lower sign for ν_μ-e^- scattering. Except where otherwise indicated, I shall use the electron's mass m_ec^2 as the unit of energy and shall adopt the value (Langacker, 1986) of $\sin^2\theta_W=0.23$. The dimensional cross-section factor is

$$\sigma_0=2G_V^2m_e^2/\pi\hbar^4=88.083\times10^{-46}\ \mathrm{cm}^2\ . \tag{11}$$

I neglect radiative corrections, which are expected to be of order several percent.

The effects of atomic binding of the electrons and of radiative and electroweak corrections are neglected in Eq. (1). One can include atomic effects by Fourier analyzing the wave function of the initial bound electron. The calculated corrections (Bahcall, 1964) are small, of order $(v/c)^2_{\mathrm{bound}}\sim(\alpha Z_{\mathrm{screened}}/n)^2$, where Z_{screened} is the effective charge on the nucleus seen by the electron and n is the principal quantum number of a hydrogeniclike orbit. The radiative and electroweak corrections are also small, of order of percent in the total cross section for MeV neutrinos (see Sarantakos, Sirlin, and Marciano, 1983).

The total cross section can be computed by analytically integrating Eq. (1) between a chosen value of $T_{\min}$ (typically several MeV in most experiments) and the maximum value $T_{\max}$ of the electron kinetic energy allowed by energy and momentum conservation:

$$T_{\max}(q)=2q^2/(1+2q)\ . \tag{12}$$

The result is

$$\sigma_{\mathrm{tot},q}(T_{\min})=\sigma_0\left[(g_L^2+g_R^2)(T_{\max}-T_{\min})-\left[\frac{g_R^2}{q}+\frac{g_Lg_R}{2q^2}\right](T_{\max}^2-T_{\min}^2)+\frac{g_R^2}{3q^2}(T_{\max}^3-T_{\min}^3)\right]\ . \tag{13}$$

The final integration over the spectrum of incoming neutrino energies q must be performed numerically. Let $P(q)$ be the *normalized* neutrino spectrum incident at Earth. Then

$$\sigma_{\mathrm{tot}}(T_{\min})=\int_0^{q_{\max}}dq\,P(q)\sigma_{\mathrm{tot},q}(T_{\min})\ . \tag{14}$$

Experimentally, the most interesting quantity is often the differential scattering cross section as a function of the recoil energy of the electron. The spectrum-averaged differential cross section is

$$\left\langle\frac{d\sigma}{dT}\right\rangle_T\equiv\int_{q_{\min}}^{q_{\max}}dq\,P(q)\frac{d\sigma}{dT}\ , \tag{15}$$

where the minimum neutrino energy that can cause an electron recoil of kinetic energy T is

$$q_{\min}(T)=\{T+[T(T+2)]^{1/2}\}/2\ . \tag{16}$$

The energy $q_{\min}$ is appropriate when the electron is scattered in the forward direction of the incoming neutrino. As a check on the numerical calculations, the total cross section can also be calculated by integrating $\langle d\sigma/dT\rangle_T$ between $T_{\min}$ and $T_{\max}$.

The angular distribution of the recoil electrons contains important information about the direction of the incoming neutrinos. For solar neutrinos, the angular distribution depends only on the cosine μ of the angle between the (instantaneous) Earth-sun axis and the momentum of the recoil electron. Since the interaction involves only two particles, one can specify either the electron's scattering angle (μ) or kinetic energy (T) for a given neutrino energy (q) or, conversely, one can determine the neutrino energy from the recoil kinetic energy and scattering angle. The relations connecting these quantities are ($T\neq0$)

$$\mu^2=\frac{T(1+q)^2}{(T+2)q^2}\ , \tag{17}$$

$$T=\frac{2q^2\mu^2}{(1+q)^2-q^2\mu^2}\ , \tag{18}$$

and

$$q(\mu)=\frac{T+|\mu|\sqrt{T(T+2)}}{(T+2)\mu^2-T}\ . \tag{19}$$

The maximum kinetic energy $T_{\max}$ is achieved at $\mu=+1$ [cf. Eqs. (12) and (18)]. The minimum value of the cosine of the scattering angle, $\mu_{\min}$, is given by Eq. (17) with $T=T_{\min}$.

The angular distribution for a fixed neutrino energy is

$$\frac{d\sigma}{d\mu}=\frac{4(1+q)^2q^2\mu}{[(1+q)^2-\mu^2q^2]^2}\left[\frac{d\sigma}{dT}\right]_{T(\mu)}, \tag{20}$$

where for a given μ and q the kinetic energy T is computed from Eq. (18) and the differential cross section for a fixed T is given by Eq. (9). The spectrum-averaged angular distribution is

$$\left\langle\frac{d\sigma}{d\mu}\right\rangle_{T_{\min}}=\int_0^{q_{\max}}dq\,P(q)\left[\frac{d\sigma}{d\mu}\right]_{T\geq T_{\min}}. \tag{21}$$

As an additional numerical check, one can calculate the total cross section by integrating $\langle d\sigma/d\mu\rangle_{T_{\min}}$ over all directions.

IV. TOTAL CROSS SECTIONS

The first question one must ask in considering any solar neutrino experiment is "What is the expected rate?" To answer this question, one needs the total interaction cross sections for all of the neutrino sources.

Table I gives the total cross sections for neutrino-electron scattering by the solar neutrino sources listed in Sec. II, as well as two possible calibration sources (^{51}Cr and ^{65}Zn). The neutrinos are assumed to be pure electron neutrinos (ν_e) or pure muon neutrinos (ν_μ) when they reach the target on Earth. (Presumably, for the calibration sources only the ν_e cross sections are experimentally relevant.) I have also listed in parentheses the changes in the cross section that are caused by a 1% change in the square of the sine of the Weinberg angle. Specifically, the numerical values in parentheses were computed by calculating the cross section at three different values for $\sin^2\theta_W$ and then evaluating the fractional change F, defined by the expression

TABLE I. Total neutrino-electron scattering cross sections for solar neutrino sources and possible calibration sources. The neutrinos are assumed to be pure ν_e or pure ν_μ when they reach the detector. The cross sections were calculated for $\sin^2\theta_W=0.23$; the quantities in parentheses are the fractional changes F in the cross sections for a change in $\sin^2\theta_W$ equal to 0.01 [see Eq. (22)]. The minimum allowed recoil kinetic energy is zero in all cases considered in this table; the maximum recoil energy is given in the third column.

Source	q (MeV)	$T_{\max}$ (MeV)	$\sigma_{e\text{-}\nu_e}$ (10^{-46} cm^2)	$\sigma_{e\text{-}\nu_\mu}$ (10^{-46} cm^2)
p-p	≤ 0.420	0.261	11.6	3.15
			(0.026)	(−0.020)
pep	1.442	1.225	112	21.7
			(+0.028)	(−0.034)
^{3}He+p	≤ 18.773	18.52	884	150
			(+0.029)	(−0.041)
^{7}Be	0.862	0.665	59.3	12.6
			(+0.028)	(−0.030)
^{7}Be	0.384	0.231	19.6	4.98
			(+0.027)	(−0.022)
^{8}B	<15.0	14.5	608	104
			(+0.029)	(−0.041)
^{13}N	≤ 1.199	0.988	46.5	10.1
			(+0.028)	(−0.029)
^{15}O	≤ 1.732	1.509	71.9	14.7
			(+0.028)	(−0.032)
^{17}F	≤ 1.740	1.517	72.2	14.7
			(+0.028)	(−0.032)
^{51}Cr	0.746	0.556	49.2	10.7
			(+0.028)	(−0.029)
^{51}Cr	0.426	0.266	22.8	5.64
			(+0.027)	(−0.023)
^{65}Zn	0.227	0.107	8.76	2.54
			(+0.026)	(−0.017)
^{65}Zn	1.343	1.128	102.5	20.2
			(+0.028)	(−0.033)
^{65}Zn	≤ 0.330	0.186	6.60	1.95
			(+0.026)	(−0.016)

$$F \equiv \frac{0.01}{\sigma}\left[\frac{d\sigma}{d\sin^2\theta_W}\right] . \quad (22)$$

The quantity F is a measure of the sensitivity of the calculated cross sections to the assumed Weinberg angle. A 1% change in the square of the sine of the Weinberg angle typically corresponds to a change of a few percent in the computed total cross sections.

Experimentally, the most accessible source of solar neutrinos is from the decay of ^{8}B. How important is it to have a low-energy threshold for counting the recoil electrons? This question is answered in Table II, which lists the total cross sections for ^{8}B solar neutrinos as a function of the minimum allowed kinetic energy of the recoil electron, $T_{\min}$.

I present results that were calculated assuming that the neutrinos which reach the Earth are either pure electron neutrinos or pure muon neutrinos. For the cutoff values of interest, the ratio of ν_e-e to ν_μ-e scattering cross sections is approximately constant,

$$\left[\frac{\sigma_{\nu_e\text{-}e}}{\sigma_{\nu_\mu\text{-}e}}\right] \approx 6\text{—}7 . \quad (23)$$

Figure 1 illustrates the strong dependence of the scattering cross section for ^{8}B neutrinos upon the threshold kinetic energy $T_{\min}$. Below 7 MeV, the effect of an incremental improvement of 1 or 2 MeV in the threshold kinetic energy is relatively moderate ($\lesssim$ a factor of 2), but in the region above 7 MeV each additional MeV reduction in the threshold significantly increases the predicted event rate. It is important, therefore, for solar neutrino experiments to have low backgrounds down to a kinetic energy of order 7 MeV (and even lower if possible).

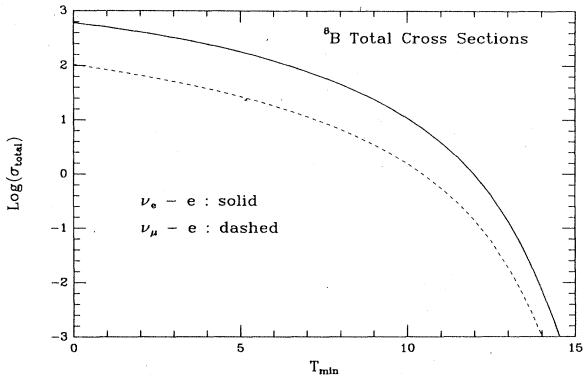

FIG. 1. ^{8}B neutrino scattering cross sections. The total cross sections for ν-e^- scattering are shown as a function of the minimum accepted electron kinetic energy $T_{\min}$. The unit of cross section is 10^{-46} cm^2. The solid curve represents the ν_e-e^- cross sections and the dashed curved represents the ν_μ-e^- cross sections.

The ^{3}He + p neutrinos are also of special interest. They would be relatively easy to detect if abundant, since the ^{3}He + p neutrinos have the highest end-point energy (18.775 MeV) of any of the appreciable neutrino sources in the standard solar model. Moreover, their abundance is likely to be increased in nonstandard solar models in which it is assumed that the temperature gradient is lower (which discriminates against the ^{8}B neutrinos) but fresh ^{3}He is mixed into the core.

Table III gives the total scattering cross sections for

TABLE II. ^{8}B neutrino scattering cross sections. The scattering cross sections for ^{8}B solar neutrinos incident on electrons are given for different values of the minimum accepted kinetic energy $T_{\min}$. The neutrinos are assumed to be pure electron neutrinos (ν_e) or muon neutrinos (ν_μ) when they reach the Earth. The cross sections were calculated for $\sin^2\theta_W = 0.23$. The quantities $F_{e\text{-}\nu_e}$ and $F_{e\text{-}\nu_\mu}$ are the fractional changes in the cross section for a change in $\sin^2\theta_W$ equal to 0.01 [see Eq. (22)].

$T_{\min}$ (MeV)	$\sigma_{e\text{-}\nu_e}$ (10^{-46} cm^2)	$F_{e\text{-}\nu_e}$	$\sigma_{e\text{-}\nu_\mu}$ (10^{-46} cm^2)	$F_{e\text{-}\nu_\mu}$
0.0	6.08×10^{2}	0.029	1.04×10^{2}	−0.040
1.0	5.09×10^{2}	0.029	8.39×10^{1}	−0.046
2.0	4.15×10^{2}	0.028	6.63×10^{1}	−0.052
3.0	3.27×10^{2}	0.028	5.10×10^{1}	−0.056
4.0	2.48×10^{2}	0.028	3.79×10^{1}	−0.060
5.0	1.80×10^{2}	0.028	2.71×10^{1}	−0.063
6.0	1.23×10^{2}	0.027	1.83×10^{1}	−0.065
7.0	7.90×10^{1}	0.027	1.16×10^{1}	−0.067
8.0	4.64×10^{1}	0.027	6.76×10^{0}	−0.068
9.0	2.44×10^{1}	0.027	3.53×10^{0}	−0.069
10.0	1.10×10^{1}	0.027	1.58×10^{0}	−0.070
11.0	3.93×10^{0}	0.027	5.64×10^{-1}	−0.070
12.0	9.88×10^{-1}	0.027	1.41×10^{-1}	−0.071
13.0	1.36×10^{-1}	0.027	1.94×10^{-2}	−0.071
13.5	3.60×10^{-2}	0.027	5.13×10^{-3}	−0.071
14.0	7.4×10^{-3}	0.027	1.0×10^{-3}	−0.071

TABLE III. ^{3}He+p neutrino scattering cross sections. The scattering cross sections for ^{3}He+p solar neutrinos incident on electrons are given for different values of the minimum accepted kinetic energy $T_{\min}$. The neutrinos are assumed to be pure electron neutrinos (ν_e) or muon neutrinos (ν_μ) when they reach the Earth. The cross sections were calculated for $\sin^2\theta_W=0.23$. The quantities $F_{e\text{-}\nu_e}$ and $F_{e\text{-}\nu_\mu}$ are the fractional changes in the cross section for a change in $\sin^2\theta_W$ equal to 0.01 [see Eq. (22)].

$T_{\min}$ (MeV)	$\sigma_{e\text{-}\nu_e}$ (10^{-46} cm^2)	$F_{e\text{-}\nu_e}$	$\sigma_{e\text{-}\nu_\mu}$ (10^{-46} cm^2)	$F_{e\text{-}\nu_\mu}$
0.0	8.84×10^{2}	0.029	1.50×10^{2}	−0.041
1.0	7.84×10^{2}	0.029	1.29×10^{2}	−0.045
2.0	6.87×10^{2}	0.029	1.10×10^{2}	−0.050
3.0	5.94×10^{2}	0.028	9.32×10^{1}	−0.053
4.0	5.04×10^{2}	0.028	7.77×10^{1}	−0.057
5.0	4.20×10^{2}	0.028	6.37×10^{1}	−0.059
6.0	3.42×10^{2}	0.028	5.12×10^{1}	−0.062
7.0	2.71×10^{2}	0.028	4.01×10^{1}	−0.064
8.0	2.09×10^{2}	0.028	3.06×10^{1}	−0.065
9.0	1.55×10^{2}	0.027	2.26×10^{1}	−0.067
10.0	1.10×10^{2}	0.027	1.59×10^{1}	−0.068
11.0	7.45×10^{1}	0.027	1.07×10^{1}	−0.069
12.0	4.71×10^{1}	0.027	6.74×10^{0}	−0.069
13.0	2.73×10^{1}	0.027	3.89×10^{0}	−0.070
13.5	1.99×10^{1}	0.027	2.84×10^{0}	−0.070
14.0	1.41×10^{1}	0.027	2.00×10^{0}	−0.071
15.0	6.11×10^{0}	0.027	8.66×10^{-1}	−0.071
16.0	2.01×10^{0}	0.027	2.85×10^{-1}	−0.071
17.0	3.88×10^{-1}	0.027	5.49×10^{-2}	−0.071
17.5	1.11×10^{-1}	0.027	1.57×10^{-2}	−0.071
18.0	1.5×10^{-2}	0.027	2.1×10^{-3}	−0.072

^{3}He + p neutrinos on electrons as a function of the threshold kinetic energy $T_{\min}$. Equation (23) again describes reasonably accurately the ratio of ν_e-e to ν_μ-e scattering cross sections. The results are illustrated in Fig. 2. By comparing Figs. 1 and 2, we see that the ^{3}He + p neutrinos are more important than the ^{8}B neutrinos for producing electron recoil energies in excess of 13.5 MeV, if, as estimated (Bahcall and Ulrich, 1987), the ratio of fluxes in the standard solar model is $\approx 10^{2.5}$. Unfortunately, the absolute cross section is small for this large cutoff energy so the hep neutrinos will only be observable if either very large detectors are used [see comment (3) of Sec. IX] or the sun is described by a nonstandard solar model.

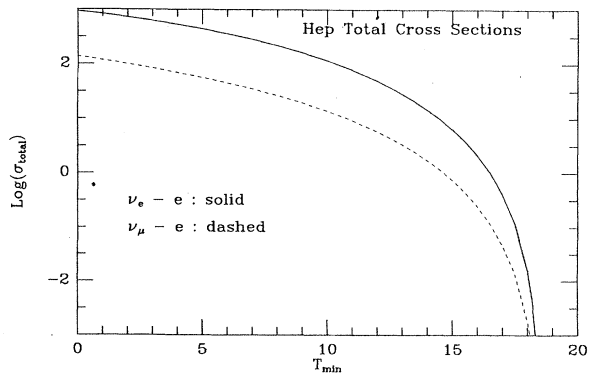

FIG. 2. ^{3}He+p neutrino scattering cross sections. The total cross sections for ν-e^- scattering are shown as a function of the minimum accepted electron kinetic energy $T_{\min}$. The unit of cross section is 10^{-46} cm^2. The solid curve represents the ν_e-e^- cross sections and the dashed curve represents the ν_μ-e^- cross sections.

V. ENERGY DISTRIBUTIONS OF RECOIL ELECTRONS

What is the energy spectrum of neutrinos that are incident on the Earth? Is that spectrum consistent with the theoretical spectrum of solar neutrinos calculated with the aid of the standard solar model and the hypothesis of nuclear fusion as the solar energy source? Is there evidence for resonant conversion of electron neutrinos to some other flavor? Is the spectrum modified by the decay of the lower-energy neutrinos? All of these questions are fundamental and subject to experimental tests. In this section I give the distributions of recoil energies that are calculated assuming the incident neutrino spectra are identical with those calculated with the aid of a standard solar model and the hypothesis of nuclear fusion. The modifications due to neutrino decay are considered in Sec. VII (see especially Fig. 14). In Sec. IX I consider more generally the information that can be derived from the recoil energy spectra (see especially Fig. 15). The recoil spectra implied by the MSW effect are given by Bahcall, Gelb, and Rosen (1987).

TABLE IV. Recoil spectrum from ν_e-e scattering by ^{8}B neutrinos. The kinetic energy of the electron is denoted by T (measured in MeV) and the normalized probability distributions per MeV by $P(T)$. Here $2.9E-02$ represents 2.9×10^{-2}.

T	$P(T)$	T	$P(T)$	T	$P(T)$	T	$P(T)$	T	$P(T)$
0.0	0.166	3.0	0.137	6.0	0.083	9.0	$2.9E-02$	12.0	$2.7E-03$
0.1	0.165	3.1	0.136	6.1	0.081	9.1	$2.7E-02$	12.1	$2.4E-03$
0.2	0.164	3.2	0.135	6.2	0.079	9.2	$2.6E-02$	12.2	$2.1E-03$
0.3	0.164	3.3	0.133	6.3	0.077	9.3	$2.5E-02$	12.3	$1.8E-03$
0.4	0.163	3.4	0.132	6.4	0.075	9.4	$2.3E-02$	12.4	$1.6E-03$
0.5	0.162	3.5	0.130	6.5	0.073	9.5	$2.2E-02$	12.5	$1.3E-03$
0.6	0.162	3.6	0.128	6.6	0.071	9.6	$2.1E-02$	12.6	$1.1E-03$
0.7	0.161	3.7	0.127	6.7	0.069	9.7	$2.0E-02$	12.7	$9.6E-04$
0.8	0.160	3.8	0.125	6.8	0.067	9.8	$1.8E-02$	12.8	$8.1E-04$
0.9	0.159	3.9	0.123	6.9	0.065	9.9	$1.7E-02$	12.9	$6.7E-04$
1.0	0.159	4.0	0.122	7.0	0.063	10.0	$1.6E-02$	13.0	$5.5E-04$
1.1	0.158	4.1	0.120	7.1	0.061	10.1	$1.5E-02$	13.1	$4.5E-04$
1.2	0.157	4.2	0.118	7.2	0.059	10.2	$1.4E-02$	13.2	$3.6E-04$
1.3	0.156	4.3	0.116	7.3	0.057	10.3	$1.3E-02$	13.3	$2.9E-04$
1.4	0.155	4.4	0.114	7.4	0.056	10.4	$1.2E-02$	13.4	$2.3E-04$
1.5	0.155	4.5	0.113	7.5	0.054	10.5	$1.2E-02$	13.5	$1.8E-04$
1.6	0.154	4.6	0.111	7.6	0.052	10.6	$1.1E-02$	13.6	$1.4E-04$
1.7	0.153	4.7	0.109	7.7	0.050	10.7	$9.9E-03$	13.7	$1.1E-04$
1.8	0.152	4.8	0.107	7.8	0.048	10.8	$9.1E-03$	13.8	$7.9E-05$
1.9	0.151	4.9	0.105	7.9	0.046	10.9	$8.4E-03$	13.9	$5.9E-05$
2.0	0.150	5.0	0.103	8.0	0.045	11.0	$7.7E-03$	14.0	$4.4E-05$
2.1	0.149	5.1	0.101	8.1	0.043	11.1	$7.0E-03$	14.1	$3.2E-05$
2.2	0.148	5.2	0.099	8.2	0.041	11.2	$6.4E-03$	14.2	$2.3E-05$
2.3	0.146	5.3	0.097	8.3	0.040	11.3	$5.8E-03$	14.3	$1.7E-05$
2.4	0.145	5.4	0.095	8.4	0.038	11.4	$5.3E-03$	14.4	$1.2E-05$
2.5	0.144	5.5	0.093	8.5	0.036	11.5	$4.8E-03$	14.5	$8.2E-06$
2.6	0.143	5.6	0.091	8.6	0.035	11.6	$4.3E-03$	14.6	$5.7E-06$
2.7	0.142	5.7	0.089	8.7	0.033	11.7	$3.8E-03$	14.7	$3.8E-06$
2.8	0.140	5.8	0.087	8.8	0.032	11.8	$3.4E-03$	14.8	$2.5E-06$
2.9	0.139	5.9	0.085	8.9	0.030	11.9	$3.0E-03$	14.9	$1.6E-06$

In order to provide sufficient detail for analyzing large-scale counter experiments (see the references cited in Sec. I), I give in Tables IV and V the probability distributions $P(T)$ for the production of recoil electrons with kinetic energies T by ν_e-e^- and ν_μ-e^- scattering by ^{8}B solar neutrinos. The results, which were obtained using Eq. (15), are illustrated in Fig. 3. The general shapes of the recoil spectra are similar in the experimentally most accessible region above a few MeV, the main difference being in the magnitude of the cross section [see Eq. (13)]. Thus the MSW effect will primarily affect the *magnitude* but not the *shape* of the recoil spectrum in the experimentally accessible region.

Although they are expected to be rare, it may be possible to detect, in experiments involving massive amounts of scattering material, the high-energy tail of the distribution of recoil electrons that are scattered by the ^{3}He + p neutrinos. This branch is of special interest since it is sensitive to different aspects of the solar model than the ^{8}B neutrinos. Tables VI and VII and Fig. 4 show the recoil spectra for ^{3}He + p neutrino-electron scattering. Again, the general shapes of the recoil spectra are similar for ν_e-e^- and ν_μ-e^- scattering, although the total cross sections are different [Eq. (13)]. The recoil electrons from ^{3}He + p neutrino-electron scattering extend about 4 MeV beyond the cutoff for electrons from scattering by ^{8}B neutrinos. The higher-energy ^{3}He + p neutrinos may make possible additional searches for solar neutrinos in some existing detectors.

The neutrinos from the p-p reaction, Eq. (1), are of fundamental importance because they provide a signature of the fusion reaction that is the basis for most of solar energy generation. Moreover, at least one proposed experiment (Cabrera *et al.*, 1985) is aimed at detecting these neutrinos. I give in Table VIII the probability distributions for both ν_e-e^- and ν_μ-e^- scattering. The results are illustrated in Fig. 5(a). For comparison, I show in Fig. 5(b) the probability distributions for the line neutrinos produced by the related pep reaction, Eq. (7). For the p-p neutrinos, the recoil spectrum falls steeply over the allowed energy range (0.0—0.26 MeV), while for the pep neutrinos the probability distribution is relatively flat over most of the allowed energy range (0.0—1.2 MeV).

In a recent discussion, Mann (1986) has proposed an important experiment to detect the 0.862-MeV line from electron capture by ^{7}Be in the sun; see Eq. (8). I show in Fig. 6(a) the calculated probability distributions for the production of recoil electrons due to scattering by the

TABLE V. Recoil spectrum from ν_μ-e scattering by ^{8}B neutrinos. The kinetic energy of the electron is denoted by T (measured in MeV) and the normalized probability distributions per MeV by $P(T)$.

T	$P(T)$	T	$P(T)$	T	$P(T)$	T	$P(T)$	T	$P(T)$
0.0	0.208	3.0	0.136	6.0	0.074	9.0	2.4E−02	12.0	2.3E−03
0.1	0.205	3.1	0.134	6.1	0.072	9.1	2.3E−02	12.1	2.0E−03
0.2	0.202	3.2	0.132	6.2	0.070	9.2	2.2E−02	12.2	1.7E−03
0.3	0.199	3.3	0.130	6.3	0.068	9.3	2.1E−02	12.3	1.5E−03
0.4	0.196	3.4	0.128	6.4	0.066	9.4	2.0E−02	12.4	1.3E−03
0.5	0.194	3.5	0.126	6.5	0.064	9.5	1.9E−02	12.5	1.1E−03
0.6	0.191	3.6	0.123	6.6	0.063	9.6	1.8E−02	12.6	9.5E−04
0.7	0.188	3.7	0.121	6.7	0.061	9.7	1.7E−02	12.7	8.0E−04
0.8	0.186	3.8	0.119	6.8	0.059	9.8	1.6E−02	12.8	6.7E−04
0.9	0.183	3.9	0.117	6.9	0.057	9.9	1.5E−02	12.9	5.6E−04
1.0	0.181	4.0	0.115	7.0	0.055	10.0	1.4E−02	13.0	4.6E−04
1.1	0.178	4.1	0.113	7.1	0.053	10.1	1.3E−02	13.1	3.7E−04
1.2	0.176	4.2	0.111	7.2	0.052	10.2	1.2E−02	13.2	3.0E−04
1.3	0.173	4.3	0.109	7.3	0.050	10.3	1.1E−02	13.3	2.4E−04
1.4	0.171	4.4	0.107	7.4	0.048	10.4	1.0E−02	13.4	1.9E−04
1.5	0.169	4.5	0.105	7.5	0.047	10.5	9.7E−03	13.5	1.5E−04
1.6	0.167	4.6	0.102	7.6	0.045	10.6	9.0E−03	13.6	1.1E−04
1.7	0.164	4.7	0.100	7.7	0.043	10.7	8.3E−03	13.7	8.7E−05
1.8	0.162	4.8	0.098	7.8	0.042	10.8	7.7E−03	13.8	6.6E−05
1.9	0.160	4.9	0.096	7.9	0.040	10.9	7.0E−03	13.9	4.9E−05
2.0	0.158	5.0	0.094	8.0	0.038	11.0	6.5E−03	14.0	3.6E−05
2.1	0.155	5.1	0.092	8.1	0.037	11.1	5.9E−03	14.1	2.7E−05
2.2	0.153	5.2	0.090	8.2	0.035	11.2	5.4E−03	14.2	1.9E−05
2.3	0.151	5.3	0.088	8.3	0.034	11.3	4.9E−03	14.3	1.4E−05
2.4	0.149	5.4	0.086	8.4	0.032	11.4	4.4E−03	14.4	9.8E−06
2.5	0.147	5.5	0.084	8.5	0.031	11.5	4.0E−03	14.5	6.8E−06
2.6	0.145	5.6	0.082	8.6	0.030	11.6	3.6E−03	14.6	4.7E−06
2.7	0.142	5.7	0.080	8.7	0.028	11.7	3.2E−03	14.7	3.2E−06
2.8	0.140	5.8	0.078	8.8	0.027	11.8	2.9E−03	14.8	2.1E−06
2.9	0.138	5.9	0.076	8.9	0.026	11.9	2.5E−03	14.9	1.4E−06

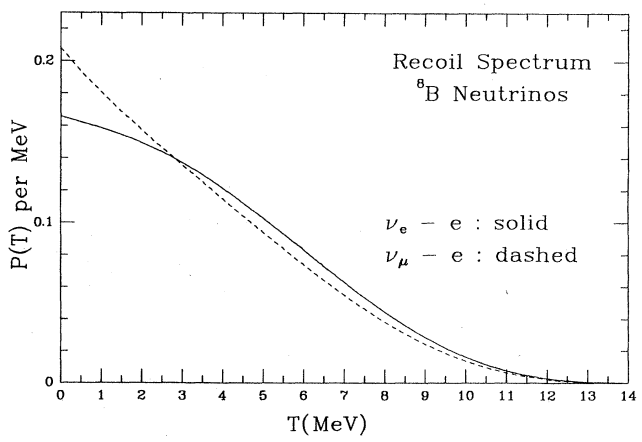

FIG. 3. Electron recoil spectrum from scattering by ^{8}B neutrinos. The probability distribution $P(T)$ of producing electrons with different recoil kinetic energies is shown as a function of the kinetic energy T. The solid curve represents the probability distribution for ν_e-e^- interactions and the dashed curve represents ν_μ-e^- interactions.

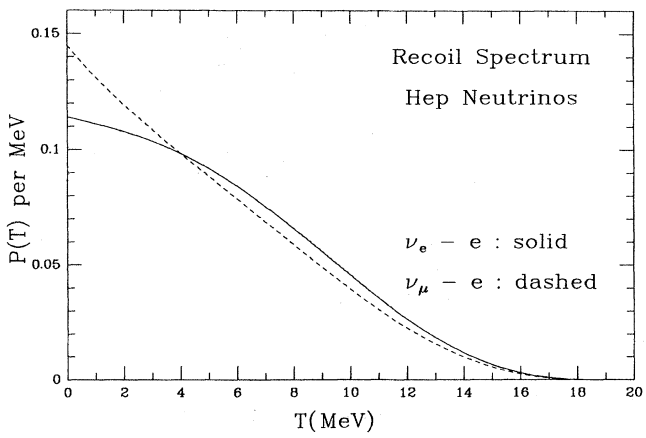

FIG. 4. Electron recoil spectrum from scattering by ^{3}He+p neutrinos. The probability distribution $P(T)$ of producing electrons with different recoil kinetic energies is shown as a function of the kinetic energy T. The solid curve represents the probability distribution for ν_e-e^- interactions and the dashed curve represents ν_μ-e^- interactions.

TABLE VI. Recoil spectrum from ν_e-e scattering by ^{3}He+p neutrinos. The kinetic energy of the electron is denoted by T (measured in MeV) and the normalized probability distributions per MeV by $P(T)$.

T	$P(T)$	T	$P(T)$	T	$P(T)$	T	$P(T)$	T	$P(T)$
0.0	0.114	3.6	0.101	7.2	0.074	10.8	3.8E−02	14.4	9.5E−03
0.1	0.114	3.7	0.100	7.3	0.073	10.9	3.7E−02	14.5	9.0E−03
0.2	0.113	3.8	0.100	7.4	0.072	11.0	3.6E−02	14.6	8.5E−03
0.3	0.113	3.9	0.099	7.5	0.071	11.1	3.5E−02	14.7	8.0E−03
0.4	0.113	4.0	0.098	7.6	0.070	11.2	3.4E−02	14.8	7.5E−03
0.5	0.113	4.1	0.098	7.7	0.069	11.3	3.3E−02	14.9	7.1E−03
0.6	0.112	4.2	0.097	7.8	0.068	11.4	3.2E−02	15.0	6.6E−03
0.7	0.112	4.3	0.097	7.9	0.067	11.5	3.1E−02	15.1	6.2E−03
0.8	0.112	4.4	0.096	8.0	0.066	11.6	3.0E−02	15.2	5.8E−03
0.9	0.111	4.5	0.095	8.1	0.065	11.7	2.9E−02	15.3	5.4E−03
1.0	0.111	4.6	0.095	8.2	0.064	11.8	2.8E−02	15.4	5.0E−03
1.1	0.111	4.7	0.094	8.3	0.063	11.9	2.8E−02	15.5	4.6E−03
1.2	0.110	4.8	0.093	8.4	0.062	12.0	2.7E−02	15.6	4.3E−03
1.3	0.110	4.9	0.093	8.5	0.061	12.1	2.6E−02	15.7	4.0E−03
1.4	0.110	5.0	0.092	8.6	0.060	12.2	2.5E−02	15.8	3.6E−03
1.5	0.109	5.1	0.091	8.7	0.059	12.3	2.4E−02	15.9	3.3E−03
1.6	0.109	5.2	0.091	8.8	0.058	12.4	2.3E−02	16.0	3.0E−03
1.7	0.109	5.3	0.090	8.9	0.057	12.5	2.2E−02	16.1	2.8E−03
1.8	0.108	5.4	0.089	9.0	0.056	12.6	2.2E−02	16.2	2.5E−03
1.9	0.108	5.5	0.088	9.1	0.055	12.7	2.1E−02	16.3	2.3E−03
2.0	0.108	5.6	0.087	9.2	0.054	12.8	2.0E−02	16.4	2.0E−03
2.1	0.107	5.7	0.087	9.3	0.053	12.9	1.9E−02	16.5	1.8E−03
2.2	0.107	5.8	0.086	9.4	0.052	13.0	1.9E−02	16.6	1.6E−03
2.3	0.107	5.9	0.085	9.5	0.051	13.1	1.8E−02	16.7	1.4E−03
2.4	0.106	6.0	0.084	9.6	0.050	13.2	1.7E−02	16.8	1.3E−03
2.5	0.106	6.1	0.083	9.7	0.049	13.3	1.6E−02	16.9	1.1E−03
2.6	0.105	6.2	0.083	9.8	0.048	13.4	1.6E−02	17.0	9.4E−04
2.7	0.105	6.3	0.082	9.9	0.047	13.5	1.5E−02	17.1	8.1E−04
2.8	0.105	6.4	0.081	10.0	0.046	13.6	1.4E−02	17.2	6.9E−04
2.9	0.104	6.5	0.080	10.1	0.045	13.7	1.4E−02	17.3	5.8E−04
3.0	0.104	6.6	0.079	10.2	0.044	13.8	1.3E−02	17.4	4.8E−04
3.1	0.103	6.7	0.078	10.3	0.043	13.9	1.2E−02	17.5	3.9E−04
3.2	0.103	6.8	0.077	10.4	0.042	14.0	1.2E−02	17.6	3.2E−04
3.3	0.102	6.9	0.076	10.5	0.041	14.1	1.1E−02	17.7	2.5E−04
3.4	0.102	7.0	0.075	10.6	0.040	14.2	1.1E−02	17.8	1.9E−04
3.5	0.101	7.1	0.074	10.7	0.039	14.3	1.0E−02	17.9	1.4E−04

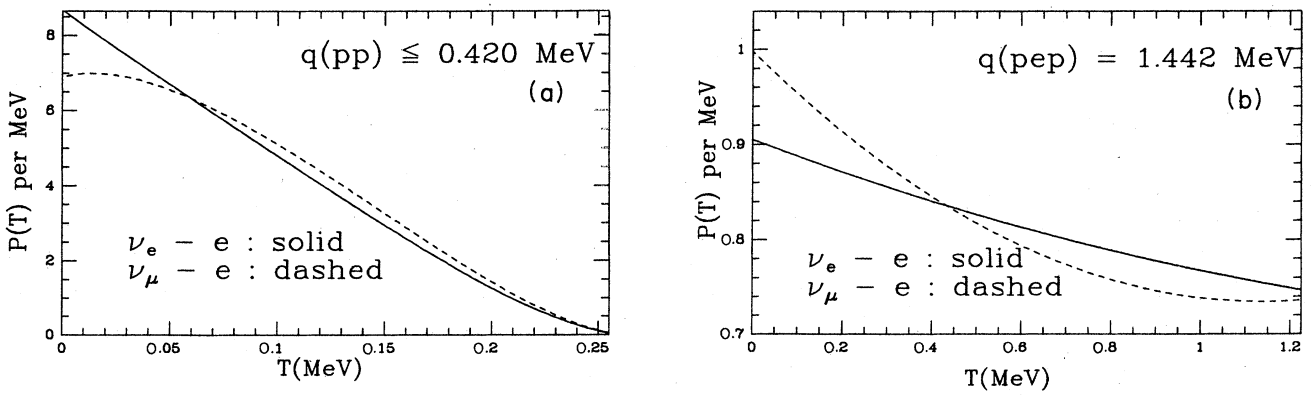

FIG. 5. Electron recoil spectrum from scattering by p-p and by p-e-p neutrinos. (a) refers to the p-p neutrinos [Eq. (1)] and (b) to the p-e-p neutrinos [Eq. (7)]. The probability distribution $P(T)$ of producing electrons with different recoil kinetic energies is shown as a function of the kinetic energy T. The solid curve represents the probability distribution for ν_e-e^- interactions and the dashed curve represents ν_μ-e^- interactions.

TABLE VII. Recoil spectrum from ν_μ-e scattering by ^{3}He+p neutrinos. The kinetic energy of the electron is denoted by T (measured in MeV) and the normalized probability distributions per MeV by $P(T)$.

T	$P(T)$	T	$P(T)$	T	$P(T)$	T	$P(T)$	T	$P(T)$
0.0	0.145	3.6	0.103	7.2	0.067	10.8	3.2E−02	14.4	8.0E−03
0.1	0.143	3.7	0.102	7.3	0.066	10.9	3.2E−02	14.5	7.6E−03
0.2	0.142	3.8	0.100	7.4	0.065	11.0	3.1E−02	14.6	7.2E−03
0.3	0.140	3.9	0.100	7.5	0.064	11.1	3.0E−02	14.7	6.7E−03
0.4	0.139	4.0	0.099	7.6	0.063	11.2	2.9E−02	14.8	6.3E−03
0.5	0.138	4.1	0.097	7.7	0.062	11.3	2.8E−02	14.9	5.9E−03
0.6	0.136	4.2	0.097	7.8	0.061	11.4	2.7E−02	15.0	5.6E−03
0.7	0.135	4.3	0.096	7.9	0.060	11.5	2.7E−02	15.1	5.2E−03
0.8	0.134	4.4	0.095	8.0	0.059	11.6	2.6E−02	15.2	4.8E−03
0.9	0.132	4.5	0.094	8.1	0.058	11.7	2.5E−02	15.3	4.5E−03
1.0	0.131	4.6	0.093	8.2	0.057	11.8	2.4E−02	15.4	4.2E−03
1.1	0.130	4.7	0.092	8.3	0.056	11.9	2.3E−02	15.5	3.9E−03
1.2	0.129	4.8	0.091	8.4	0.055	12.0	2.3E−02	15.6	3.6E−03
1.3	0.127	4.9	0.090	8.5	0.054	12.1	2.2E−02	15.7	3.3E−03
1.4	0.126	5.0	0.089	8.6	0.053	12.2	2.1E−02	15.8	3.0E−03
1.5	0.125	5.1	0.088	8.7	0.052	12.3	2.0E−02	15.9	2.8E−03
1.6	0.124	5.2	0.087	8.8	0.051	12.4	2.0E−02	16.0	2.5E−03
1.7	0.123	5.3	0.086	8.9	0.050	12.5	1.9E−02	16.1	2.3E−03
1.8	0.122	5.4	0.085	9.0	0.049	12.6	1.8E−02	16.2	2.1E−03
1.9	0.120	5.5	0.084	9.1	0.048	12.7	1.8E−02	16.3	1.9E−03
2.0	0.119	5.6	0.083	9.2	0.047	12.8	1.7E−02	16.4	1.7E−03
2.1	0.118	5.7	0.082	9.3	0.046	12.9	1.6E−02	16.5	1.5E−03
2.2	0.117	5.8	0.081	9.4	0.045	13.0	1.6E−02	16.6	1.3E−03
2.3	0.116	5.9	0.080	9.5	0.044	13.1	1.5E−02	16.7	1.2E−03
2.4	0.115	6.0	0.079	9.6	0.043	13.2	1.4E−02	16.8	1.0E−03
2.5	0.114	6.1	0.078	9.7	0.042	13.3	1.4E−02	16.9	9.2E−04
2.6	0.113	6.2	0.077	9.8	0.041	13.4	1.3E−02	17.0	7.8E−04
2.7	0.112	6.3	0.076	9.9	0.040	13.5	1.3E−02	17.1	6.8E−04
2.8	0.111	6.4	0.075	10.0	0.040	13.6	1.2E−02	17.2	5.8E−04
2.9	0.110	6.5	0.074	10.1	0.039	13.7	1.2E−02	17.3	4.9E−04
3.0	0.109	6.6	0.073	10.2	0.038	13.8	1.1E−02	17.4	4.0E−04
3.1	0.108	6.7	0.072	10.3	0.037	13.9	1.0E−02	17.5	3.3E−04
3.2	0.107	6.8	0.071	10.4	0.036	14.0	9.9E−03	17.6	2.7E−04
3.3	0.106	6.9	0.070	10.5	0.035	14.1	9.5E−03	17.7	2.0E−04
3.4	0.105	7.0	0.069	10.6	0.034	14.2	9.0E−03	17.8	1.6E−04
3.5	0.104	7.1	0.068	10.7	0.033	14.3	8.5E−03	17.9	1.2E−04

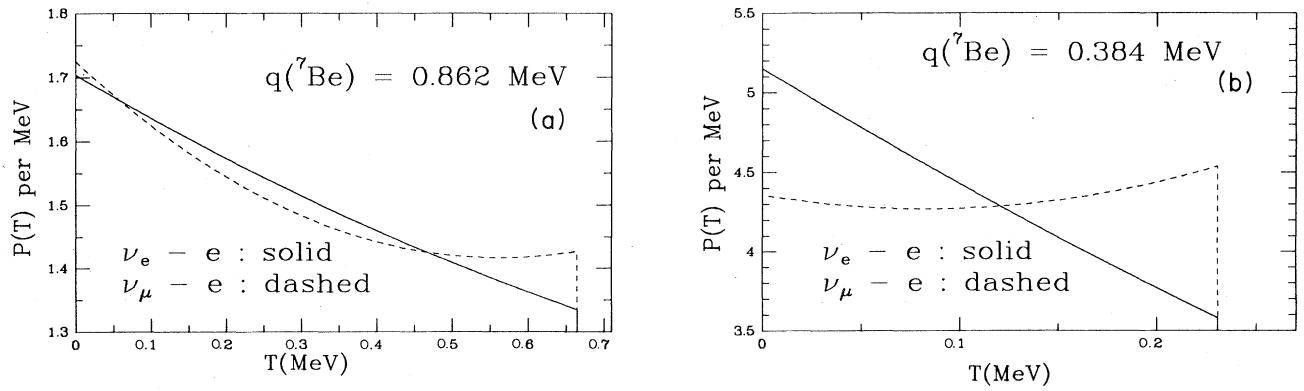

FIG. 6. Electron recoil spectrum from scattering by ^{7}Be neutrinos. (a) refers to the neutrino line with energy 0.862 MeV and (b) to the line of energy 0.384 MeV. The probability distribution $P(T)$ of producing electrons with different recoil kinetic energies is shown as a function of the kinetic energy T. The solid curve represents the probability distribution for ν_e-e^- interactions and the dashed curve represents ν_μ-e^- interactions.

TABLE VIII. Electron recoil spectrum from scattering by p-p neutrinos. The kinetic energy of the electron is denoted by T (measured in MeV) and the normalized probability distributions per MeV by $P(T)$.

T	$P(T)_{\nu_e}$	$P(T)_{\nu_\mu}$
0.000	8.6882	6.8750
0.101	8.2602	6.9883
0.020	7.8558	6.9768
0.030	7.4608	6.8862
0.040	7.0742	6.7426
0.050	6.6891	6.5476
0.060	6.3058	6.3132
0.070	5.9252	6.0487
0.080	5.5442	5.7544
0.090	5.1641	5.4371
0.100	4.7861	5.1022
0.110	4.4063	4.7466
0.120	4.0309	4.3822
0.130	3.6546	4.0034
0.141	3.2869	3.6254
0.151	2.9213	3.2403
0.161	2.5669	2.8618
0.171	2.2196	2.4850
0.181	1.8812	2.1134
0.191	1.5545	1.7511
0.201	1.2487	1.4103
0.211	0.9604	1.0869
0.221	0.6938	0.7864
0.231	0.4541	0.5152
0.241	0.2482	0.2819
0.251	0.0903	0.1026

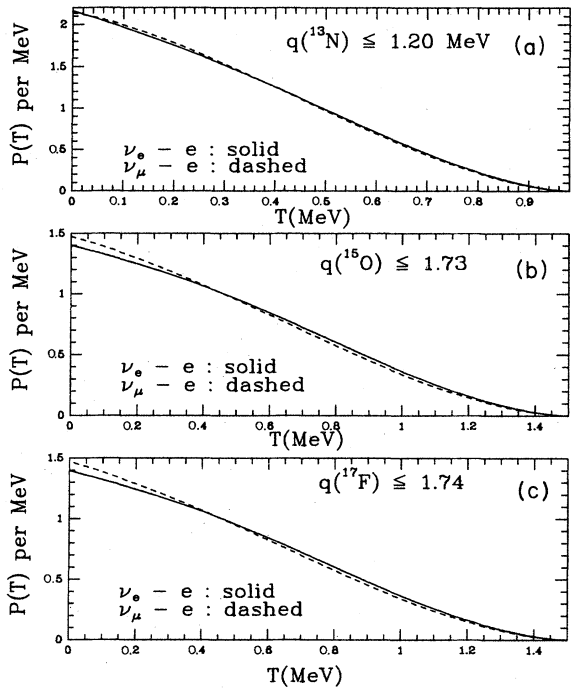

FIG. 7. Electron recoil spectrum from scattering by ^{13}N, ^{15}O, and ^{17}F neutrinos. (a) shows the recoil spectrum from interactions with neutrinos having a ^{13}N spectrum and (b) and (c) show the essentially identical results from interactions with neutrinos having ^{15}O and ^{17}F spectra. The probability distribution $P(T)$ of producing electrons with different recoil kinetic energies is shown as a function of the kinetic energy T. The solid curve represents the probability distribution for ν_e-e^- interactions and the dashed curve represents ν_μ-e^- interactions.

0.862-MeV neutrino line and in Fig. 6(b) the corresponding probabilities for the associated 0.384-MeV ^{7}Be line. Note the qualitatively different shapes of the recoil spectra, which reflect the different values of the energy of the neutrino lines [cf. Eq. (8)].

For electron recoil energies below 1 MeV, a number of different solar neutrino sources can produce electrons in a given energy. To calculate the expected spectrum from the standard solar model, one must add together the recoil distributions from all of the important neutrino sources [Eqs. (1)—(8)] with the weights determined by detailed solar-model calculations of the individual neutrino fluxes. I therefore show in Figs. 7(a) and 7(b) the recoil distributions that are appropriate to ^{13}N, ^{15}O, and ^{17}F solar neutrinos [Eqs. (4)—(6)].

VI. ANGULAR DISTRIBUTIONS OF RECOIL ELECTRONS

The angular distribution of the recoil electrons is strongly peaked in the forward direction of the Earth-sun axis. A convenient analytic formula representing this forward peaking is given by Bahcall (1964). I present here the detailed angular distributions that are calculated using Eq. (21) and the solar neutrino spectra that were discussed in Sec. II.

In order to summarize the results quantitatively, it is convenient to define a critical scattering angle θ_c, such that 90% of the recoil electrons are scattered within a cone of half-opening angle θ_c about the forward direction of the Earth-sun axis. Table IX gives the value of θ_c for both ^{8}B and ^{3}He + p solar neutrino spectra. The computed values of θ_c depend sensitively upon the minimum electron energy $T_{\min}$ that is accepted in a given experimental arrangement. If *all* of the recoil electrons are counted ($T_{\min}=0.0$ MeV), the angular distributions are rather broad (half-opening angle in excess of 45°). However, for the larger values of $T_{\min}$, the angular distributions are strongly forward peaked. Typical opening angles are $\theta_c \approx 15°$ for a 5-MeV threshold and $\theta_c \approx$ a few degrees for the highest-energy electrons. Table IX shows that the values of θ_c are very similar for scattering by electron and muon neutrinos except when very low thresholds are used.

There is an interesting competition between different physical effects that is expressed in the results shown in

TABLE IX. Angle within which 90% of the electrons are scattered. The minimum kinetic energy of the electron is denoted by $T_{\min}$ (measured in MeV) and the angle within which 90% of the electrons are scattered is represented by θ_c (in degrees). The second and third columns were computed using a ^{8}B neutrino spectrum and the fourth and fifth columns were calculated with a ^{3}He$+p$ neutrino spectrum.

$T_{\min}$ (MeV)	θ_{c,ν_e} ^{8}B	θ_{c,ν_μ} ^{8}B	θ_{c,ν_e} ^{3}He$+p$	θ_{c,ν_μ} ^{3}He$+p$
0.0	48.26	51.44	43.62	47.05
1.0	33.00	33.98	32.18	33.45
2.0	25.38	25.89	25.76	26.45
3.0	20.60	20.90	21.53	21.96
4.0	17.20	17.40	18.44	18.75
5.0	14.60	14.74	16.07	16.29
6.0	12.51	12.60	14.16	14.32
7.0	10.76	10.82	12.56	12.68
8.0	9.25	9.29	11.18	11.27
9.0	7.92	7.94	9.98	10.04
10.0	6.71	6.72	8.90	8.94
11.0	5.61	5.61	7.93	7.95
12.0	4.58	4.58	7.03	7.04
13.0	3.69	3.69	6.18	6.19
14.0	2.97	2.97	5.36	5.37

Table IX. As expected, the higher-energy ^{3}He $+ p$ neutrinos, which on the average are more energetic than the ^{8}B neutrinos [cf. Eqs. (2) and (3)], are more strongly peaked in the forward direction if all recoil electrons are accepted (i.e., $T_{\min}=0.0$ MeV). This is an expression of the well-understood phenomenon that forward scattering predominates in the laboratory frame at high energies because the center-of-mass frame is moving strongly forward in the laboratory frame. However, for values of $T_{\min} \geq 3$ MeV, the higher-energy ^{3}He $+ p$ neutrinos produce a more spread-out angular distribution (cf. Table IX). The reason is that neutrinos with larger energies q can scatter electrons to bigger angles for a given fixed value of $T_{\min}$. The larger the scattering angle (the smaller the value of the cosine μ), the smaller is the value of the electron recoil energy [see Eq. (18)]. One can easily understand this effect from the fact that as $T_{\min}$ approaches the maximum value allowed by energy conservation, $T_{\max}$, all of the electrons are scattered in the forward direction. Since $(T_{\max})_{^3\text{He}+p} > (T_{\max})_{^8\text{B}}$, at the largest values of $T_{\min}$ shown in Table IX the ^{8}B neutrinos scatter electrons nearly all in the forward direction, whereas the ^{3}He $+ p$ neutrinos are energetic enough to produce some electrons at larger angles.

Figures 8 and 9 illustrate the results described above

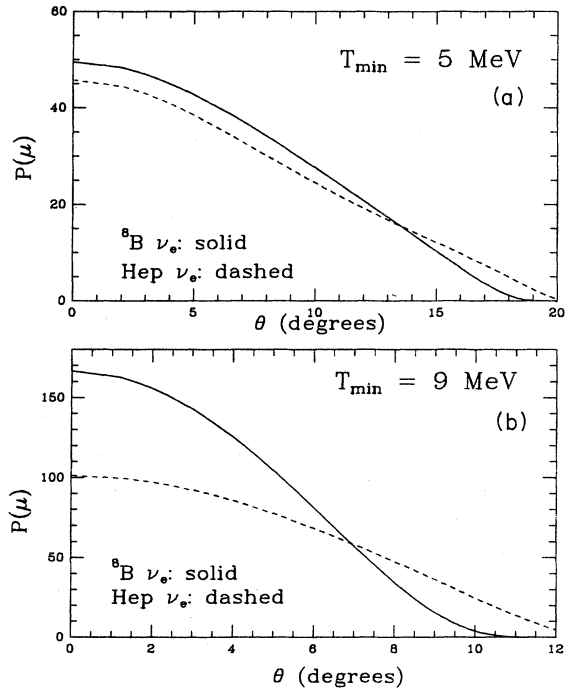

FIG. 8. Angular distributions for ^{8}B and ^{3}He$+p$ neutrinos. Here $P(\mu)$ is the differential probability per unit of cosine ($d\mu$) for an electron to be scattered to an angle θ. The solid curves represent the probability distributions for ^{8}B neutrinos and the dashed curves represent the scattering probabilities for ^{3}He$+p$ neutrinos. Results are shown for two typical values of $T_{\min}$, 5 and 9 MeV.

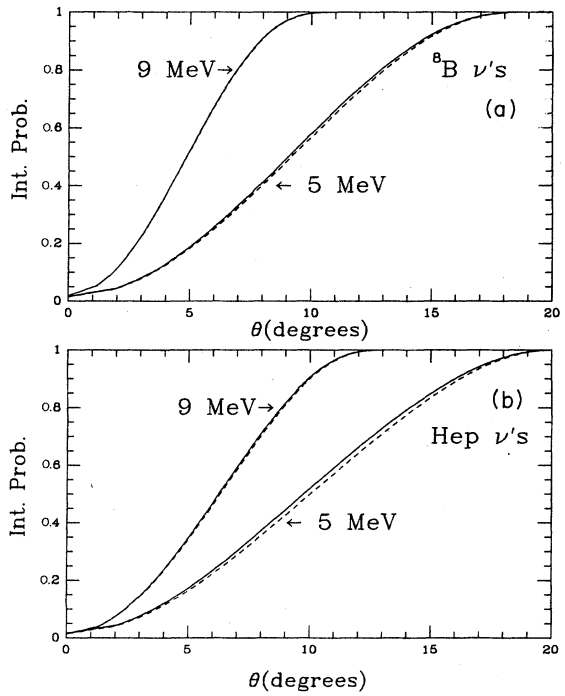

FIG. 9. Integral probabilities for angular distributions of ^{8}B and ^{3}He$+p$ neutrinos. Here, Int. Prob. is the integrated probability for an electron to be scattered to any angle less than or equal to θ. The solid curves represent the probabilities for electron neutrinos and the dashed curves represent the probabilities for muon neutrinos. (a) refers to scattering by neutrinos with a ^{8}B neutrino spectrum and (b) refers to scattering by a ^{3}He$+p$ neutrino spectrum. Results are shown for two typical values of $T_{\min}$, 5 and 9 MeV.

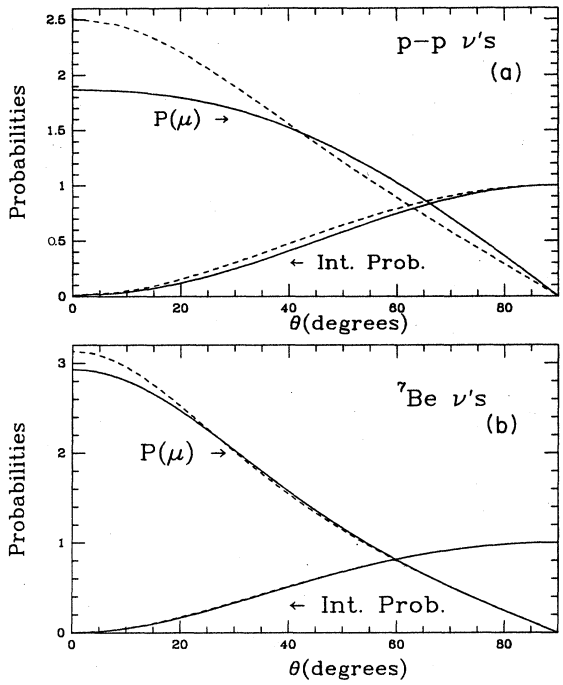

FIG. 10. Angular distributions for p-p and ^{7}Be neutrinos. (a) refers to the p-p neutrinos and (b) pertains to neutrinos with an energy of 0.862 MeV [^{7}Be neutrinos, cf. Eq. (8)]. Here $P(\mu)$ is the differential probability per unit of cosine ($d\mu$) for an electron to be scattered to an angle θ and Int. Prob. is the integrated probability distribution. The solid curves represent the probability distributions for electron neutrinos and the dashed curves represent the scattering probabilities for muon neutrinos.

and give the detailed angular distributions for both ^{8}B and ^{3}He + p electron neutrinos. Figure 8 shows the detailed angular distributions for electron neutrinos for two typical values of $T_{\min}$, namely, 5 and 9 MeV. As described in the preceding paragraph, the higher-energy ^{3}He + p neutrinos have a broader angular distribution in both cases. Figure 9 gives the *integral* probability distributions for electrons to be scattered within different angles, again for the same two values of $T_{\min}$. In Fig. 9 I have plotted separately the integral angular distributions for electron neutrinos and for muon neutrinos; the differences are barely visible

Figure 10 illustrates the broad angular distributions that are expected from two low-energy sources of neutrinos, the p-p neutrinos and the ^{7}Be (0.862 MeV) neutrinos. I show both the differential and the integral probability distributions. Note that the differences between ν_e and ν_μ are somewhat more pronounced for these low-energy sources.

VII. NEUTRINO DECAY

The sun provides a beam of low-energy neutrinos that can be used to explore characteristics of the weak interaction that are inaccessible with terrestrial experiments. One of the possible applications of solar neutrino experiments is to test the stability of neutrinos over extremely long proper times. If the origin of the solar neutrino problem is decay on the way to the Earth from the sun, then a 10-MeV electron neutrino has a mean decay lifetime of abut 5×10^2 s (Bahcall, Cabibbo, and Yahil, 1972; Bahcall, Petcov, Toshev, and Valle, 1986). If this is the case, only the ^{8}B and ^{3}He + p solar neutrinos reach the Earth in sufficient quantities to be measurable. The terrestrial flux of solar neutrinos of energy q (in MeV), φ_{decay}, is decreased exponentially relative to the flux that would be present if there were no decay, φ_{stable}, according to the relation

$$\frac{\varphi_{\text{decay}}}{\varphi_{\text{stable}}} = \exp[-(10\ \text{MeV}/q)]\ . \tag{24}$$

Figure 11 compares the original energy spectrum of ^{8}B neutrinos, normalized to unit probability, with the spectrum that reaches the Earth after partially decaying in transit. The most apparent difference in the spectra is in the total number of neutrinos: only 21% of the neutrinos that leave the sun reach the Earth. The ^{8}B neutrino spectrum that is modified by decay has its peak shifted to a somewhat higher energy, 8.2 MeV, than the peak of the original spectrum, which occurs at 6.4 MeV. The full width at half-maximum of the spectrum after decay is somewhat narrower, 3.4 MeV, than the 4 MeV of the original spectrum. These changes in the shape of the spectrum caused by decay are relatively modest, although the difference in the total flux is decreased by a factor of almost 5. We therefore anticipate that the total cross sections for electron-neutrino scattering will be decreased significantly by decay, although the change in the spectrum shape will be less dramatic.

Table X and Figs. 12—14 demonstrate the expected trends. Table X gives the total electron-neutrino scattering cross sections for both ^{8}B and ^{3}He+p neutrino spec-

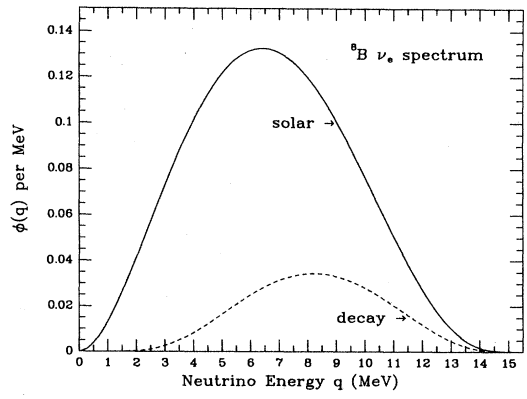

FIG. 11. Energy spectra of ^{8}B solar neutrinos with and without decay. The solid (upper) curve is the normalized spectrum of neutrinos produced at the sun and the dashed (lower) curve is the spectrum that would be observed at the Earth if a 10-MeV electron neutrino has a mean life of 5×10^2 s.

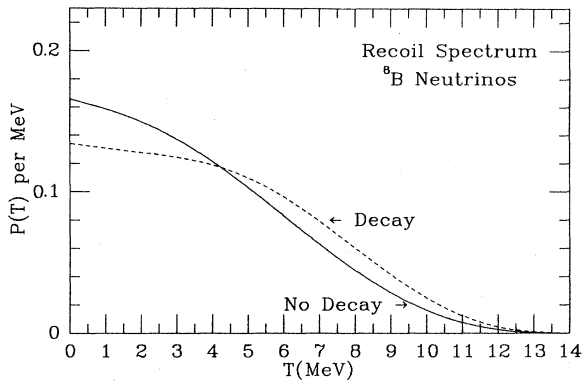

FIG. 12. Effect of neutrino decay on the electron recoil spectrum from scattering by ^{8}B neutrinos. The solid curve represents the recoil spectrum that was calculated assuming no decay occurs and the dashed curve is the spectrum calculated assuming decay occurs according to Eq. (24). The probability distribution $P(T)$ of producing electrons with different recoil kinetic energies is shown as a function of the kinetic energy T.

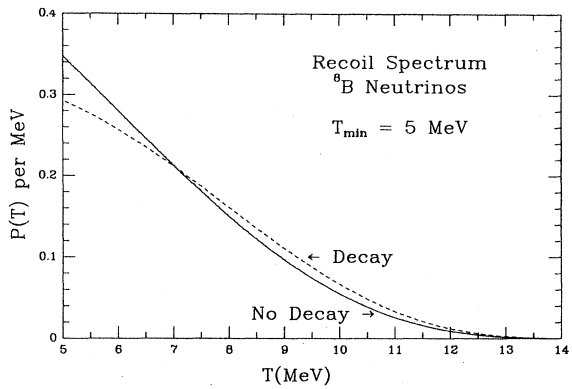

FIG. 14. Comparison of decay and nondecay spectra for $T_{min}=5$ MeV. Only electrons with kinetic energy greater than 5 MeV are considered here. The solid curve represents the recoil spectrum that was calculated assuming no decay occurs and the dashed curve is the spectrum calculated assuming decay occurs according to Eq. (24). The probability distribution $P(T)$ of producing electrons with different recoil kinetic energies is shown as a function of the kinetic energy T.

tra modified by decay according to Eq. (24). By comparison with Tables II and III, we see that neutrino decay decreases the expected event rate for ^{8}B neutrinos (values for ^{3}He$+p$ neutrinos in parentheses) by factors of 3.8 (2.6), 3.0 (2.3), and 2.4 (2.1), respectively, for $T_{min}=0$, 5, and 9 MeV. The effect of neutrino decay on the *total* event rate is therefore sufficiently large that a $3-\sigma$ difference should be apparent with only $\sim 10^2$ events.

The effect of neutrino decay on the shape of the energy spectra of the recoil electrons is shown in Figs. 12–14 and is not nearly as pronounced. Figure 12 gives the *separately normalized* probability distributions to produce recoil electrons of kinetic energies T for both decaying and nondecaying ^{8}B neutrinos. The recoil spectrum in the case of decaying neutrinos is shifted to somewhat higher energies, although the general shape of the curves is not very dissimilar. Figure 13 compares decay and nondecay recoil spectra for ^{3}He$+p$ neutrinos, with similar results. In order to indicate what might be feasible in a practical experiment, I show in Fig. 14 the recoil spectrum with incident ^{8}B neutrinos and a minimum-accepted kinetic energy of 5 MeV.

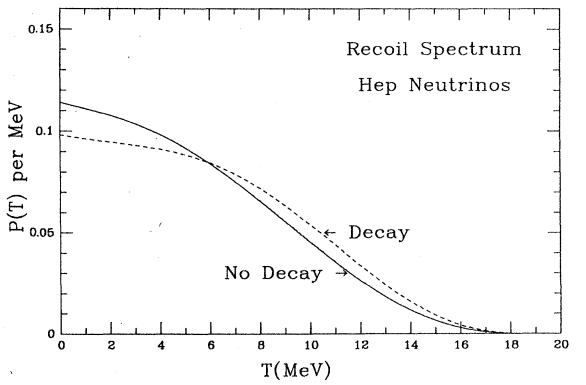

FIG. 13. Effect of neutrino decay on the electron recoil spectrum from scattering by ^{3}He$+p$ neutrinos. The solid curve represents the recoil spectrum that was calculated assuming no decay occurs and the dashed curve is the spectrum calculated assuming decay occurs according to Eq. (24). The probability distribution $P(T)$ of producing electrons with different recoil kinetic energies is shown as a function of the kinetic energy T.

TABLE X. Effect of decay on neutrino scattering cross sections. The scattering cross sections for ^{8}B and ^{3}He$+p$ solar neutrinos (ν_e) incident on electrons are given for different values of the minimum accepted kinetic energy T_{min}. The neutrino spectra are assumed affected by decay according to the relation given in Eq. (24).

T_{min} (MeV)	$\sigma(^8\text{B})$ 10^{-46} cm^2	$\sigma(^3\text{He}+p)$ 10^{-46} cm^2
0.0	1.6E+02	3.4E+02
1.0	1.4E+02	3.1E+02
2.0	1.2E+02	2.8E+02
3.0	1.0E+02	2.4E+02
4.0	8.0E+01	2.1E+02
5.0	6.1E+01	1.8E+02
6.0	4.4E+01	1.5E+02
7.0	3.0E+01	1.2E+02
8.0	1.8E+01	9.8E+01
9.0	1.0E+01	7.5E+01
10.0	4.8E+00	5.4E+01
11.0	1.8E+00	3.8E+01
12.0	4.6E−01	2.4E+01
13.0	6.6E−02	1.4E+01
13.5	1.8E−02	1.1E+01
14.0	3.7E−03	7.6E+00

To demonstrate experimentally the somewhat subtle changes in the recoil spectra that are indicated in Figs. 12—14, a total number of events of order 10^3 or more would be required.

VIII. CROSS SECTIONS AT SPECIFIC ENERGIES

For many purposes, it is convenient to have available numerical values for neutrino-electron scattering cross sections at specific energies. Table XI gives the computed cross sections for neutrino energies ranging from 1 to 60 MeV. The tabulated values were determined for $T_{\min}=0.0$ MeV. I have neglected radiative corrections, which are significant for the larger energies.

The recoil spectrum for ν_e-e scattering is relatively flat [see Eq. (9)]. Therefore, for ν_e-e scattering, the cross sections given in Table XI can be used to estimate reasonably accurately the cross section for a specified minimum recoil electron energy. One simply multiplies the tabulated values by $(T_{\max}-T_{\min})/T_{\max}$. This approximation is less appropriate for ν_μ-e scattering, but still will give a useful first estimate.

IX. DISCUSSION AND CONCLUSIONS

I summarize in this section the main results that are described in the preceding sections and make some comments on the implications of these results for future solar neutrino experiments.

(1) Flavor dependence. Electron neutrinos have larger cross sections than muon neutrinos by a typical factor of order 6 or 7 [see Eq. (23)] for the higher-energy ^{8}B and ^{3}He+p neutrino spectra if the minimum-accepted electron recoil energy $T_{\min}$ is above several MeV. Thus the event rate for an electron-scattering detector is sensitive to neutrino flavor. Neutrino-electron scattering experiments, when combined with absorption experiments that measure the incident beam of ν_e's, can test effectively whether or not electron neutrinos have been resonantly converted to neutrinos of a different flavor (the MSW effect).

(2) Total cross sections. The total cross sections for the sources of interest are given in Tables I—III. The cross sections depend strongly upon the minimum recoil energy $T_{\min}$ (see Fig. 1). This is especially true for thresholds larger than 7 MeV. For each MeV that the threshold is lowered, the expected counting rate increases significantly. It is important, therefore, that solar neutrino experiments have low backgrounds down to an electron kinetic energy of order 7 MeV (even lower values are desirable) so that $T_{\min}$ may be set as low as possible.

The expected event rate in the Icarus (^{40}Ar) experiment is rather large by the standards of underground experiments. The number of scattering events from ^{8}B solar neutrinos with $T_{\min}=5$ MeV is 10^3 per kiloton per year if the flux of electron neutrinos has the value given by the standard solar model (6×10^6 cm^{-2}s^{-1}). If the ν_e's are converted to ν_μ's, then the event rate is reduced by a factor of about 7 (see Table II). Thus a kiloton experiment with liquid argon should provide a decisive test of whether or not the MSW effect occurs (for a more extensive discussion of this point, see Bahcall, Baldo-Ceolin, Cline, and Rubbia, 1986).

(3) Hep neutrinos. Electron recoil energies above $\sim$13.5 MeV are produced almost entirely by neutrinos from the rare ^{3}He+p reaction. Therefore the energy range between 13.5 and 18.5 MeV can be used to study the solar reaction ^{3}He+p [Eq. (2)], which is rather broadly distributed in the sun (Bahcall and Ulrich, 1987) (unlike the ^{8}B neutrinos, which are produced mainly in the innermost few percent of the solar mass). The event rate will be rather small if the standard solar model is correct, only of order 0.15 events with $\geq$13.5 MeV per kiloton of argon per year. Fortunately, however, the ^{3}He+p reaction is sensitive to the assumptions of some of the nonstandard solar models (especially the mixing of ^{3}He) and could be much larger in some of the models. Therefore hep neutrinos can provide a useful diagnostic of the stellar physics once the hep flux is calculated in the various nonstandard solar models. The fact that a ^{3}He+p neutrino spectrum produces some recoil electrons with higher energies than is possible with ^{8}B neutrinos may enable additional underground experiments to be used as solar neutrino detectors.

(4) Electron recoil spectra. The detailed electron recoil spectra are given in Tables IV—VIII for ^{8}B, ^{3}He+p, and p-p neutrinos and in Figs. 3—7 for all the important sources. Unfortunately, the predicted shapes of the recoil spectra are not sensitive to neutrino flavor in the experimentally most accessible region above a few MeV. Thus the MSW effect primarily changes the magnitude of the

TABLE XI. Scattering cross sections for individual neutrino energies. The tabulated values were computed for $T_{\min}=0.0$ MeV.

q (MeV)	$\sigma_{\nu_e\text{-}e}$ (10^{-46} cm^2)	$\sigma_{\nu_\mu\text{-}e}$ (10^{-46} cm^2)
1.0	7.15E+01	1.48E+01
2.0	1.63E+02	3.05E+01
3.0	2.57E+02	4.62E+01
4.0	3.51E+02	6.18E+01
5.0	4.45E+02	7.75E+01
7.0	6.35E+02	1.09E+02
10.0	9.19E+02	1.56E+02
12.0	1.11E+03	1.87E+02
14.0	1.30E+03	2.18E+02
16.0	1.49E+03	2.49E+02
18.0	1.68E+03	2.80E+02
20.0	1.87E+03	3.12E+02
25.0	2.34E+03	3.90E+02
30.0	2.82E+03	4.68E+02
40.0	3.77E+03	6.24E+02
50.0	4.71E+03	7.80E+02
60.0	5.66E+03	9.36E+02

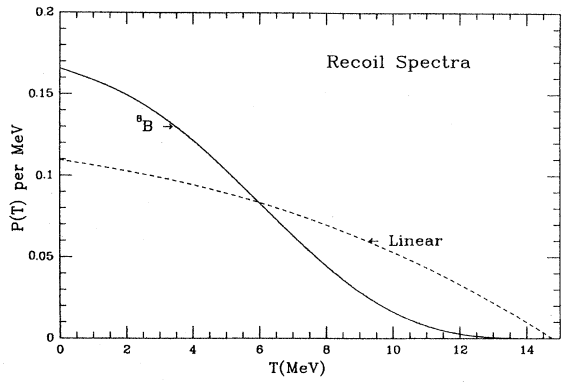

FIG. 15. Comparison of recoil distributions from linear and ^{8}B neutrino spectra. The solid curve represents the probability distribution for scattering by a ^{8}B neutrino spectrum and the dashed curve represents the probability distribution for scattering by a fictitious linear spectrum [cf. Eq. (25)]. The probability distribution $P(T)$ of producing electrons with different recoil kinetic energies is shown as a function of the kinetic energy T.

scattering cross section and has relatively little effect on the shape of the recoil spectrum. This result may seem surprising at first since the MSW effect does have a dramatic effect on the flavor content of the incident neutrino spectrum (see, e.g., Mikheyev and Smirnov, 1986, Rosen and Gelb, 1986, and Bethe, 1986). However, the energy dependence of the scattering cross sections is relatively insensitive to the flavor of the incident neutrinos [see Eq. (9) and Figs. 3—7].

How sensitive is the observed recoil spectrum to the incident neutrino *energy spectrum*? Figure 15 provides a specific answer to this question. I compare in Fig. 15 the recoil electron spectra that were calculated with two different assumed neutrino spectra: (1) the theoretical ^{8}B neutrino spectrum (the solid curve in Fig. 11) and (2) a *fictitious* linear neutrino spectrum,

$$P(q)=\frac{2q}{q^2_{\max}} . \tag{25}$$

For simplicity, the flavor of both spectra was assumed to be pure ν_e. The recoil spectrum calculated for the fictitious linear spectrum is shown as a dashed line in Fig. 15 and is very different from the recoil distribution that is predicted for a ^{8}B neutrino spectrum (the solid line in Fig. 15). *I conclude that measurements of the recoil electron energy spectrum can provide a consistency test for the predictions of solar models and of neutrino physics.*

(5) Angular distributions. The higher-energy electrons are strongly forward peaked in the direction of the Earth-sun axis. For electrons with energies above 5 MeV, 90% of the electrons are scattered into a cone with an opening angle of 15° about the forward direction, and this critical scattering angle decreases to just a few degrees for the highest-energy electrons. If lower-energy electrons are accepted, the angular distribution is rather broad. The general results are given in Table IX as a function of $T_{\min}$. Figures 8—10 illustrate the expected angular distributions for electrons scattered by p-p, ^{7}Be, ^{8}B, and ^{3}He+p neutrinos.

(6) Neutrino decay. If neutrino decay is the correct solution of the solar neutrino problem, then the shape, and especially the amplitude, of the neutrino spectrum that reaches the Earth is very different from what it is when the neutrinos leave the sun. Figure 11 shows a comparison of the solar and the decay-modified neutrino spectra. If consistency is required with the observed ^{37}Cl capture rate, then neutrino decay decreases the scattering rate for ν_e-e^- interactions by about a factor of 3 (depending somewhat upon the specific threshold $T_{\min}$, see Table X). Thus a relatively modest experiment, which accumulated only $\sim 10^2$ events (corresponding to ~ 0.1 kilton of liquid argon counted for about a year), should be able to establish at a $5-\sigma$ level of significance the depressed rate that is implied by the hypothesis of neutrino decay. The effect of decay upon the *shape* of the recoil energy spectrum is shown in Figs. 12—14 and is less pronounced. To detect experimentally the differences shown in Figs. 12—14 would require $\sim 10^3$ scattering events (~ 1 kilton of liquid argon for a year).

ACKNOWLEDGEMENT

This work was supported in part by the National Science Foundation.

REFERENCES

Arisaka, K., *et al.*, 1985, J. Phys. Soc. Jpn. **54**, 3213.
Badino, G., *et al.*, 1984, Nuovo Cimento **7C**, 573.
Bahcall, J. N., 1964, Phys. Rev. **136**, 1164B.
Bahcall, J. N., 1978, Rev. Mod. Phys. **50**, 881.
Bahcall, J. N., M. Baldo-Ceolin, D. B. Cline, and C. Rubbia, 1986, Phys. Lett. B **178**, 324.
Bahcall, J. N., N. Cabibbo, and A. Yahil, 1972, Phys. Rev. Lett. **28**, 316.
Bahcall, J. N., and R. Davis, 1976, Science **191**, 264.
Bahcall, J. N., and R. Davis, 1982, in *Essays in Nuclear Astrophysics,* edited by C. A. Barnes, D. D. Clayton, and D. N. Schramm (Cambridge University Press, Cambridge, England) p. 243.
Bahcall, J. N., and S. C. Frautschi, 1969, Phys. Lett. B **29**, 263.
Bahcall, J. N., J. Gelb, and S. P. Rosen, 1987, Phys. Rev. D **35**, 2976.
Bahcall, J. N., W. F. Heubner, W. H. Lubow, P. D. Parker, and R. K. Ulrich, 1982, Rev. Mod. Phys. **54**, 767.
Bahcall, J. N., and B. R. Holstein, 1986, Phys. Rev. C **33**, 2121.
Bahcall, J. N., S. T. Petcov, S. Toshev, and J. W. F. Valle, 1986, Phys. Lett. B **181**, 369.
Bahcall, J. N., and R. K. Ulrich, 1987 (in preparation).
Bakich, A. M., and L. S. Peak, 1985, in *Solar Neutrinos and Neutrino Astronomy,* AIP Conference Proceedings No. 126, edited by M. L. Cherry, W. A. Fowler, and K. Lande (AIP, New York), p. 238.
Barabanov, I. R., *et al.*, 1985, in *Solar Neutrinos and Neutrino Astronomy,* AIP Conference Proceedings No. 126, edited by M.

L. Cherry, W. A. Fowler, and K. Lande (AIP, New York), p. 175.
Bethe, H. A., 1986, Phys. Rev. Lett. **56**, 1305.
Cabrera, B., L. M. Krauss, and F. Wilczek, 1985, Phys. Rev. Lett. **55**, 25.
Chen, H. H., 1985, Phys. Rev. Lett. **55**, 1534.
Cline, D. L., 1985, in *Solar Neutrinos and Neutrino Astronomy,* AIP Conference Proceedings No. 126, edited by M. L. Cherry, W. A. Fowler, and K. Lande (AIP, New York), p. 295.
Cowan, G. A., and W. C. Haxton, 1982, Science **216**, 51.
Cribier, M., W. Hampel, J. Rich, and D. Vignaud, 1986, Saclay Report No. DPHPE 86-17.
Dar, A., A. Mann, Y. Melina, and D. Zajfman, 1987, Phys. Rev. D (in press).
Davis, R., Jr., 1986, *Report to the Seventh Workshop on Grand Unification, ICOBAN '86,* Toyoma, Japan (Japanese Press, Tokyo).
Gribov, V., and B. Pontecorvo, 1969, Phys. Lett. B **28**, 495.
Hampel, W., 1985, in *Solar Neutrinos and Neutrino Astronomy,* AIP Conference Proceedings No. 126, edited by M. L. Cherry, W. A. Fowler, and K. Lande (AIP, New York), p. 162.
Hurst, G. S., C. H. Chen, S. D. Kramer, B. T. Cleveland, R. Davis, Jr., R. K. Rowley, Fletcher Gabbard, and F. J. Schima, 1984, Phys. Rev. Lett. **53**, 1116.
Langacker, P., 1986, *Proceedings of the International Symposium on Weak and Electromagnetic Interactions in Nuclei, Heidelberg* (Springer, Heidelberg).
Mann, A. K., 1987, in Proceedings of the 1986 Summer Study on the Physics of the Superconducting Super Collider, Snowmass, Colorado, 1986.
Mikheyev, S. P., and A. Yu. Smirnov, 1986, Nuovo Cimento **9C**, 17.
Raghavan, R. S., 1978, in "Proceedings of the Informal Conference on the Status and Future of Solar Neutrino Research," edited by G. Friedlander, Brookhaven National Laboratory Report No. 50879, Vol. 2, p. 1.
Reines, F., and W. R. Kropp, 1964, Phys. Rev. Lett. **12**, 457.
Rosen, S. P., and J. Gelb, 1986, Phys. Rev. D **34**, 969.
Sarantakos, S., A. Sirlin, and W. J. Marciano, 1983, Nucl. Phys. B **217**, 84.
't Hooft, G., 1971, Phys. Lett. B **37**, 195.
Warburton, E. K., 1986, Phys. Rev. C **33**, 303.
Wilkinson, D. H., and D. E. Alburger, 1971, Phys. Rev. Lett. **26**, 1127.
Wolfenstein, L., 1978, Phys. Rev. D **17**, 2369.